DEVELOPMENT AND VALIDATION OF A COMPUTATIONAL MODEL FOR PREDICTING THE BEHAVIOR OF PLUMES FROM LARGE SOLID ROCKET MOTORS

Jason E. Wells[a], David L. Black[b] and Casey L. Taylor[c]
[a] *Environmental Services*
[b] *Aerothermal Analysis*
[c] *Composite Structures*
ATK Aerospace Group, Brigham City, Utah

Exhaust plumes from large solid rocket motors fired at ATK's Promontory test site carry particulates to high altitudes and typically produce deposits that fall on regions downwind of the test area. As populations and communities near the test facility grow, ATK has become increasingly concerned about the impact of motor testing on those surrounding communities. To assess the potential impact of motor testing on the community and to identify feasible mitigation strategies, it is essential to have a tool capable of predicting plume behavior downrange of the test stand. A software package, called PlumeTracker, has been developed and validated at ATK for this purpose. The code is a point model that offers a time-dependent, physics-based description of plume transport and precipitation. The code can utilize either measured or forecasted weather data to generate plume predictions. Next-Generation Radar (NEXRAD) data and field observations from twenty-three historical motor test fires at Promontory were collected to test the predictive capability of PlumeTracker. Model predictions for plume trajectories and deposition fields were found to correlate well with the collected dataset.

INTRODUCTION

Static tests of large solid rocket motors at ATK's Promontory, Utah test facility generate large exhaust plumes that can rise to high altitudes and travel several miles downrange. The plumes contain particulate matter from exhaust products and material eroded from the flame trench downstream of the motor nozzle. As the exhaust plume rises, it entrains surrounding air and forms a cloud. Once the cloud stabilizes, the particulate load falls out as either dry deposition or precipitation. An example of this behavior is shown in Figure 1, which shows the motor plume shortly after ignition; and in Figure 2, where the precipitation from the cloud base after firing is clearly evident.

Several computational models have been developed to describe transport characteristics of different types of smoke plumes. Many of the models use the equations developed by Briggs to predict the rise height of smokestack plumes [1,2,3]. The equations are widely used and define the well-known '2/3 law' for plume rise. The Briggs equations have been modified several times to be applicable for different types of plumes. Mills [4] and Fisher [5] modified the Briggs formula to take into account the initial diameter of plumes from pool fires. Cunningham [6] has shown that high-fidelity large eddy simulation (LES) calculations for forest fire plumes tend to fall in between plume heights calculated by the original and modified Briggs equations. Another approach to modeling plume rise behavior is that used in the Daysmoke code developed by Achtemeier et al. [7,8,9]. To track plume rise, Daysmoke uses an entraining turret method. In this method, a rising plume is described as a series of turrets that progressively sweep out a three-dimensional volume of surrounding air.

This work was performed under NASA Contract No: NNM07AA75C MOD 95FWD

Figure 1. Typical Motor Firing into Hill Behind T-97 Showing Motor Exhaust and Particulates Shortly After Start

Figure 2. Precipitating Cloud and Debris Trail Produced by a Five-Segment Motor Tested at T-97

Of the plume models available, the Rocket Exhaust Effluent Diffusion Model (REEDM) is the most applicable to predicting the behavior of exhaust plumes generated by large solid rocket motors [10]. REEDM is a Gaussian dispersion model developed to predict downwind concentrations of exhaust products in ground clouds generated during rocket launches. The REEDM code uses the Briggs formula to calculate plume rise and assumes uniform wind. Recently, a multi-layer model was developed around the concepts of the REEDM code [11].

However, none of the available models have been able to adequately capture the characteristics of plumes generated during large solid rocket motor tests. First, the Briggs plume rise formulas assume the plume encounters a uniform wind. Static test plumes can achieve heights greater

than 20,000 ft above sea level. Analysis of historical radiosonde data shows that static test plumes can encounter significant wind shear during ascent. These changes in wind direction can have a substantial influence on the final trajectory of the plume. Second, it is not necessary for most plume models to include the effect of condensation and precipitation on plume behavior. However, the altitude reached by large motor static test plumes often induces cloud formation and precipitation. This process results in the particulate rain that can be experienced downwind. Due to these unique factors, a new model was developed specifically to predict the trajectory and deposition field of plumes generated during static tests of large solid rocket motors.

MODEL DESCRIPTION

PlumeTracker models the processes of plume motion, cloud formation, and precipitation starting from an altitude of 6,000 ft mean sea level. **Figure 3** shows a diagram of the physical processes and associated information that must be tracked. Initial conditions for the plume model at this altitude are derived from detailed computational fluid dynamics (CFD) flow models of the motor firing into the hillside [12]. The initial plume motion is characterized following the procedure outlined by Wu and Koh [13]. The methodology outlined was modified to allow for a variable wind speed with altitude and expanded to a three-dimensional model.

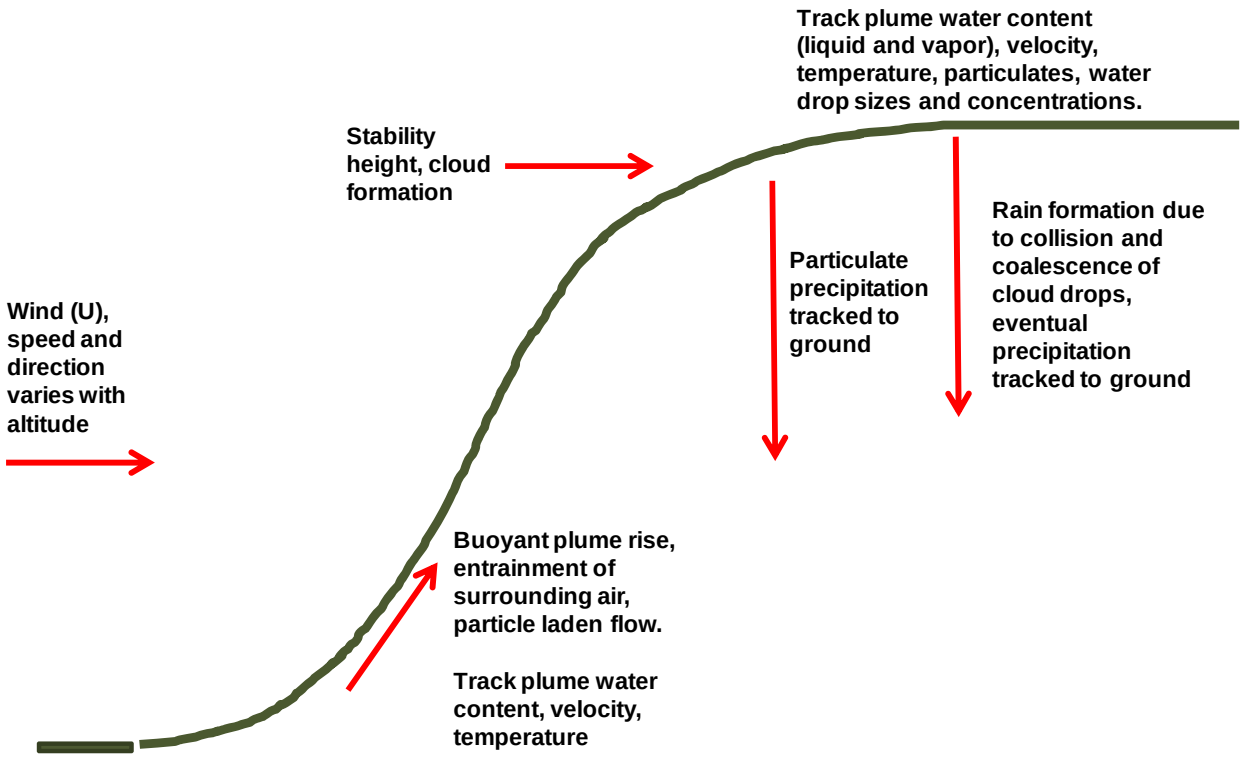

Figure 3. Plume Phenomena Captured by PlumeTracker

Wind speed and direction can be taken either from data or from weather predictions. Plume motion is tracked as a function of time by solving the conservation of mass, momentum, and

energy equations. Conservation of mass includes entrainment of ambient air and is calculated from:

$$\frac{d(A\rho_p U_p)}{ds} = \rho_a 2\pi r U_{ent} \tag{1}$$

where A is the plume cross-sectional area, ρ_p is the plume density, U_p is the plume velocity along its track, r is the plume radius, s is the direction of the plume motion, and U_{ent} is the entrainment velocity. **Figure 4** shows a diagram illustrating the plume variables and coordinates used in PlumeTracker.

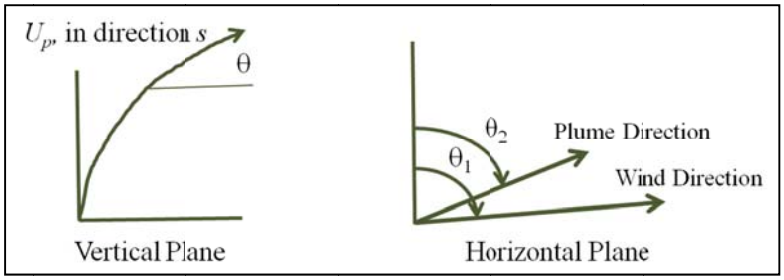

Figure 4. Plume Coordinate System and Variables

The entrainment of air into the plume as it rises is a function of the plume geometry, the plume velocity, and the local ambient conditions. The complex processes of entrainment into the plume are characterized by:

$$U_{ent} = (e_{1.1} + e_{1.2}\sin(\theta))\left|U_p - U_\infty \cos(\theta)\right| + e_2 U_\infty \left|\sin(\theta)\right| \cos(\theta) + U'_\infty U_\infty \tag{2}$$

where the e coefficients are empirically determined, U_∞ is the wind velocity in the horizontal plane, and θ is the plume tilt angle. The first term in this expression accounts for the entrainment of air into the plume due to shear forces acting along the plume boundaries. The second term accounts for air moving through the plume perpendicular to its direction of motion. Finally, the last term accounts for turbulent mixing effects along the boundary of the plume. The coefficients used in PlumeTracker are $e_{1.1}$ = 0.0806, $e_{1.2}$ = 0.6753, e_2 = 0.3, and U'_∞ = 0.05 (atmospheric turbulent intensity). These values correspond to coefficients derived for Gaussian plumes as described by Wu and Koh [13].

The plume velocities are calculated by solving a set of momentum equations as a function of distance along the plume track. The conservation equations are always taken to be in the plane of plume motion. Differences in the wind direction introduce a perpendicular component of motion that is also tracked. The resulting three-dimensional momentum equations describing the plume motion can be written as follows:

$$\frac{d(A\rho_p U_{p'}^2)}{ds} = \rho_a U_\infty \sin(\theta_1 - \theta_2) 2\pi r U_{ent} + \frac{1}{2} C_d \rho_a \left[U_\infty \sin(\theta_1 - \theta_2)\right]^2 r \tag{3}$$

$$\frac{d(A\rho_p U_p^2 \cos\theta)}{ds} = \rho_a U_\infty \cos(\theta_1 - \theta_2) 2\pi r U_{ent} + \frac{1}{2} C_d \rho_a \left[U_\infty \cos(\theta_1 - \theta_2) \sin\theta\right]^2 r |\sin\theta| \quad (4)$$

$$\frac{d(A\rho_p U_p^2 \sin\theta)}{ds} = gA(\rho_a - \rho_p(1-\sigma_p)) + \frac{1}{2} C_d \rho_a \left[U_\infty \cos(\theta_1 - \theta_2) \sin\theta\right]^2 r \cos\theta \quad (5)$$

The first term in Equations 3 and 4 accounts for the momentum of the entrained air in the horizontal plane. Buoyancy effects are accounted for in the vertical velocity momentum equation (Equation 5). Each of the momentum equations include a drag force term of the wind acting on the plume. The discharge coefficient, C_d, in each of these equations is empirically determined for the plume type being modeled. For PlumeTracker, the value used is 0.5, which is the same as that used by Wu and Koh [13] for cooling tower plumes. The plume and ambient air velocity directions in the horizontal plane are θ_1 and θ_2.

Conservation of energy is characterized through the use of the dry and wet adiabatic lapse rates. The lapse rate describes the change in plume temperature (T_p) as the volume of gas expands or is compressed. Equation 6 gives the temperature change of the plume along the plume track as a function of ambient conditions, plume motion, and the lapse rate (Γ).

$$\frac{d\left[(T_p - T_a)U_p\right]}{ds} = -\left(\frac{dT_a}{dz} + \Gamma\right) U_p \sin\theta \quad (6)$$

The lapse rate for a dry plume is 0.01 ºC/m while the wet adiabatic lapse rate [14] is calculated from:

$$\Gamma_w = g \frac{1 + \frac{H_v r}{R_{sd} T}}{C_{pd} + \frac{H_v^2 r \varepsilon}{R_{sd} T^2}} \quad (7)$$

where g is gravity, H_v is the heat of vaporization, r is the ratio of the mass or water vapor to the mass of dry air, T is temperature, R_{sd} = 287 J/kg-K, and ε = 0.622.

As the plume rises, relative humidity (RH) increases. Eventually RH increases beyond 100% and the plume is supersaturated. At this point, cloud droplets form. Cloud droplets form from condensation nuclei. Since rocket motor plumes contain high amounts of particulates, there are large numbers of potential nuclei available for cloud formation. Not all particles form cloud droplets. In the precipitation model implemented in PlumeTracker, the amount of nuclei that activate at a given supersaturation is described using the Twomey relationship [15].

$$N_{ccn} = C(100S)^k \quad (7)$$

Where N is the number/m^3 of active particles, S is supersaturation, and C and k are both empirical coefficients. Values used in PlumeTracker are C = 4000 and k = 2, which correspond

to typical values used in the literature for dirty air. This relationship has found wide usage in the literature and is featured in many models of cloud and rain formation. In the time marching algorithm used in PlumeTracker, the additional number of activated particles for each time step is found by tracking the maximum supersaturation seen and, when $S>S_{max}$, calculating the added activated droplets as:

$$\Delta N = C(100S)^k - C(100S_{\max})^k \tag{8}$$

This process is described in detail by Grabowski et al. [16]. In addition to the number of droplets capable of growing into cloud droplets, a size is also needed. Particle size as a function of supersatuation is derived from Kohler curves. A detailed description of this process is given in Rogers and Yau [17]. The Kohler curve gives a critical size beyond which the droplet will continue to grow. The critical particle radius is given by:

$$r_{act} = \frac{2}{3}\frac{A}{S}, A = \frac{2M_w\sigma_w}{RT\rho_w} \tag{9}$$

The coefficient A is calculated from water properties for molecular weight (M_w), surface tension (σ_w), and density (ρ_w). In practice, the plume radius estimated from a circular cross-section based on the area A determined from Equation 2 is used to determine the peak supersaturation at the top of the plume. Precipitation processes start to occur when some fraction of the plume is above the saturation point. Extraction of water from the plume into droplets is limited to what would be needed to bring the peak supersatuation back to one during each time step.

A binned scheme is used to track droplets, particles, and the interactions between them. At each time step, any new droplets created using the Twomey activation law and Kohler curves are added to a new bin. Dust particles are also distributed into bins and tracked along with the cloud droplets. The size and quantity of dust material carried by the plume is a user input typically based on soil composition and measured erosion. Particles are carried by the plume until the majority of the particles in each bin fall below the plume centerline. The criteria used, for both liquid and solid particles, are:

$$\int_0^t (U_p - U_f)dt = \sqrt{\frac{A_p}{\pi}} \tag{10}$$

When the relationship defined by Equation 10 is satisfied, more than half the particles have left the plume. At this point, all particles of that size are tracked to the starting elevation (6,000 ft) and used to create the precipitation track. Precipitation is spread uniformly using the radius of the cloud at the time the particle size class leaves.

When the plume becomes supersaturated, liquid drops are placed in the binned tracking scheme and the growth processes related to both condensation and collision are allowed to take place. Large dirt particles being tracked are assumed to be wetted and grow the same way that water droplets do. Condensational growth is described by the equation:

$$\frac{dR}{ds} = \frac{\xi_1(S-1)}{R}, \xi_1 = growth\ parameter \tag{11}$$

At each time step, each bin is allowed to grow as described by Equation 11. The growth parameter is calculated from a curve fit to a chart of the parameter given by Rogers and Yau [17]. Along with condensational growth, collisional growth of each bin also takes place. Collisional growth describes the process of large droplets absorbing smaller droplets due to relative velocity differences between the sizes. In integral form, the equation representing the growth of a drop due to collision is:

$$\frac{dR}{ds} = \frac{\pi}{3}\int_0^R \left(\frac{R+r}{R}\right)^2 [u_R - u_r] N_r r^3 E_{R,r} dr \tag{12}$$

N_r is the number density of particle size r and $E_{R,r}$ is the collisional efficiency of drop size R with another size r. The efficiency is derived from curve fits to the data shown in Rogers and Yau [17]. In a binned format, Equation 12 can be written as a summation of bin with size R with all smaller size bins as shown below.

$$\frac{\Delta R}{\Delta s} = \frac{\pi}{3}^2 \sum_{i=1}^{n} \left(\frac{R+r_i}{R}\right) [u_R - u_{r,i}] N_{r,i} r_i^3 E_{R,r,i} \tag{13}$$

PlumeTracker generates a Keyhole Markup Language (KML) file that is viewable with Google Earth. The track of the predicted plume movement is projected from the ground to equilibrium height. Also contained within the file are overlay images to visualize the deposition field. Dispersion calculations are also output to the KML file, if selected by the user. Dispersion tracks display as lines and are color coded by altitude.

VALIDATION DATA

A thorough literature review of validation methods for plume models was conducted. Light detection and ranging (LiDAR) and/or radar are often used to detect forest fire smoke plumes [18]. LiDAR observations provide detailed information on plume trajectory, dimensions, and particulate characteristics. These detailed plume observations have been used to validate performance of plume models developed to predict the trajectory of forest fire smoke [19,20]. However, there was no historical dataset of this type available for rocket motor static test plumes. NEXRAD can also provide a great deal of information on plume trajectory and approximate dimensions. Additionally, NEXRAD provides information on where precipitation is occurring. Although designed for weather monitoring, NEXRAD was shown to be capable of detecting the solid rocket plume of a Delta II launch failure at Cape Canaveral Air Force Station [21]. A search of local NEXRAD data found that static test motor plumes could be detected with reasonably good resolution.

Two NEXRAD facilities are capable of detecting plume signatures from large motor static tests. KMTX is located approximately 26 miles southwest of the Promontory test facilities and provides near-field plume signatures. KMTX provides archived data from December 1995 to present. KSFX is located 88 miles north of the test facilities and provides far-field signatures. KSFX provides data products from September 1995 to present. Generally, the combination of data products from both sites provides the most complete mosaic of a plume. NEXRAD data was obtained from the National Oceanic and Atmospheric Administration's (NOAA) National

Climatic Data Center [22]. Data was visualized using NOAA's Weather and Climate Toolkit [23]. The Toolkit translates NEXRAD data into KML files that can be viewed in Google Earth.

A full record of all large motor static tests conducted at Promontory test facilities from 1995 through 2011 was obtained and organized into a database suitable for validation. The record included both four-segment and five-segment rocket motors tested to support the Space Shuttle and Ares/Space Launch System programs, respectively. Twenty-two motors were fired since the radars became operational. The list of motors, the test stand location, and the available NEXRAD data are shown in Table 1. All available data was obtained from KMTX and KSFX for each motor. However, in some cases, radar data may have only been available from one of the stations. Also, in a few cases, the plume did not ascend high enough for the KSFX station to produce a signature.

Table 1. Historical Static Tests with NEXRAD Data Available

Test Date	Test ID	Test Stand	KMTX Data	KSFX Data
November 9, 1995	FSM-5	T-24	YES	NO
April 24, 1997	FSM-6	T-97	YES	YES
June 24, 1998	FSM-7	T-97	YES	YES
February 17, 2000	FSM-8	T-97	YES	YES
May 24, 2001	FSM-9	T-97	YES	YES
November 1, 2001	ETM-2	T-24	YES	YES
January 23, 2003	FSM-10	T-24	YES	YES
October 23, 2003	ETM-3	T-97	YES	YES
June 10, 2004	FSM-11	T-97	YES	YES
February 17, 2005	FVM-1	T-24	YES	NO
August 16, 2005	PRM-1	T-97	YES	YES
March 9, 2006	TEM-12	T-24	YES	YES
April 28, 2006	FSM-12	T-97	YES	YES
November 16, 2006	FSM-13	T-97	YES	YES
May 24, 2007	FSM-14	T-97	YES	YES
November 1, 2007	TEM-13	T-24	YES	YES
May 1, 2008	FVM-2	T-24	YES	YES
December 4, 2008	FSM-15	T-24	YES	YES
September 10, 2009	RSRMV DM-1	T-97	NO	YES
February 25, 2010	FSM-17	T-24	YES	YES
August 31, 2010	RSRMV DM-2	T-97	YES	YES
September 8, 2011	RSRMV DM-3	T-97	YES	YES

Plume signatures were distinct and easy to decipher for most of the historical firings. In two cases, FSM-8 and FSM-10, thunderstorms created significant background making it difficult to follow the plume track for an extended period. Even in these cases, the data was sufficient to use for comparison with PlumeTracker predictions. Data for the FSM-4 plume was taken from a plume characterization study performed for the Utah Department of Environmental Quality, Air

Quality Division [24]. The data provided sufficient detail on plume track, dimensions, and deposition/precipitation (D/P) events.

Two sources of weather data were used for plume track predictions for historical motor static tests. Radiosonde data collected from weather balloon releases was available for tests conducted since 2008. Typically, the dataset provided key parameters of interest through an altitude of 30,000 ft. Parameters of interest at a given altitude are wind direction, wind speed, relative humidity, temperature, and barometric pressure. Data is collected by the radiosonde every 100 ft during ascent. When radiosonde data was not available, "forecasts" for test day weather conditions were created. Generally, forecasts were created using archived weather balloon soundings from Salt Lake City International Airport. Upper-level wind data was somewhat limited in some of the forecast datasets. Usually, data was available for altitudes between 16,000 to 20,000 ft. Additionally, forecast data featured lower resolution relative to Promontory radiosonde data collections. Forecast data was reported in 1,000 ft intervals. Even with these drawbacks, no datasets were so limited that PlumeTracker could not generate a reasonable prediction. Still, radiosonde data was the preferred source of weather data, when available.

RESULTS AND DISCUSSION

Using either Promontory radiosonde or estimated weather data, a PlumeTracker prediction was generated for each of the historical test fires. PlumeTracker predictions were analyzed in Google Earth version 6.0.1.2032. KML files from KMTX and KSFX were overlaid on the PlumeTracker results. Plume trajectory was compared by animating the NEXRAD data and determining the deviation, if any, shown by the PlumeTracker centerline trajectory. Comparisons of predicted plume stabilization heights with the heights of signatures recorded by the radar were also made. Precipitation events were analyzed by comparing PlumeTracker precipitation predictions with radar reflectivity intensities. **Figure 5** shows the PlumeTracker prediction for DM-2 overlaid with KMTX and KSFX radar signatures. The predicted plume trajectory appears in the center of the multiple radar scans. Additionally, the heaviest projected deposition (red/yellow) on the ground correlates well with the highest reflectivity intensities (yellow/green) detected by the radar. **Figure 6** shows the PlumeTracker prediction for DM-1. The predicted trajectory cuts through the center of the radar signatures. Also, the radar's lowest scan angle picks up the low intensity reflection of diminishing precipitation falling from the plume. The low intensity signature correlates well with the end of PlumeTracker's predicted precipitation field.

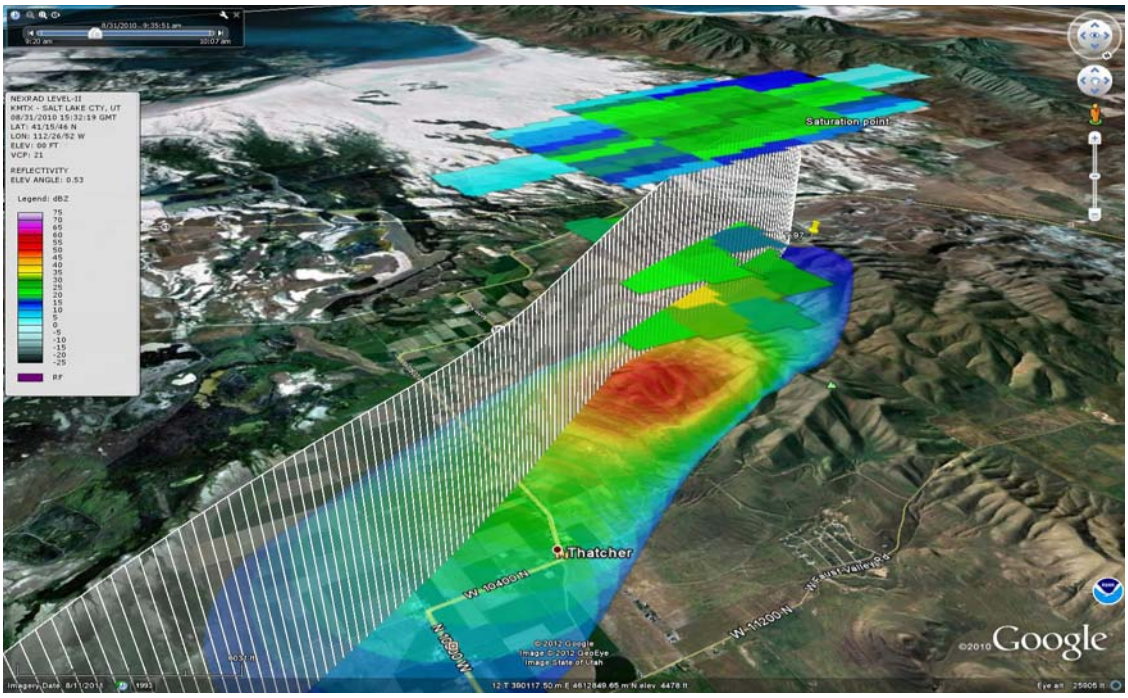

Figure 5. DM-2 PlumeTracker Prediction with KMTX and KSFX Overlay

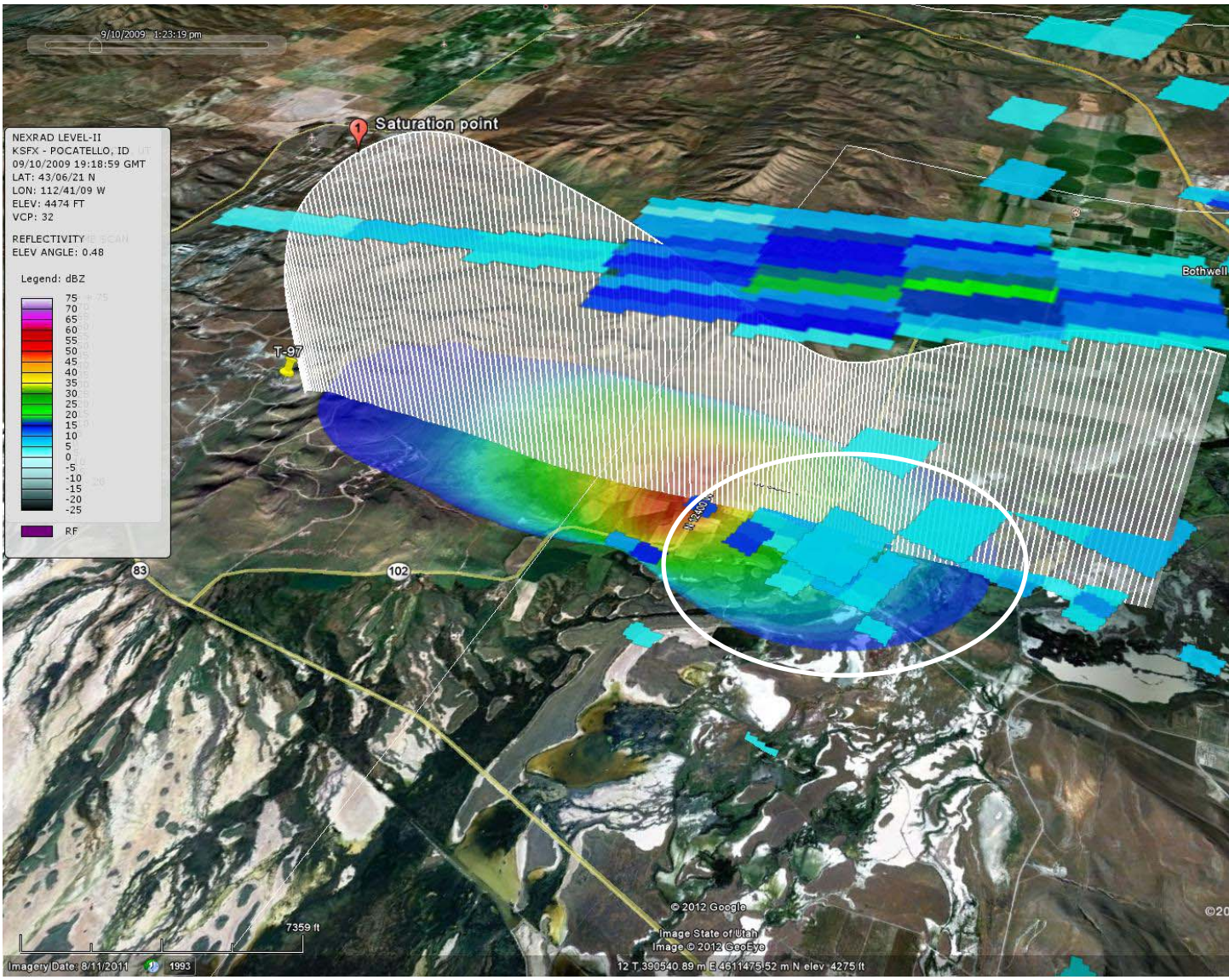

Figure 6. Diminishing Precipitation Signal from DM-1 Correlates with the End of PlumeTracker's Predicted Precipitation Field

Each predicted plume trajectory was compared to NEXRAD plume signatures to determine the level of correlation. Correlations were grouped into three levels: high, medium, and low. A high level of correlation was defined as a predicted plume trajectory that transected the majority of the radar signatures produced by NEXRAD during the timeframe the plume was visible (**Figure 7**). A moderate level of correlation was defined as a trajectory that transected early radar signatures but clearly began to deviate as the plume moved downrange. A low level of correlation was

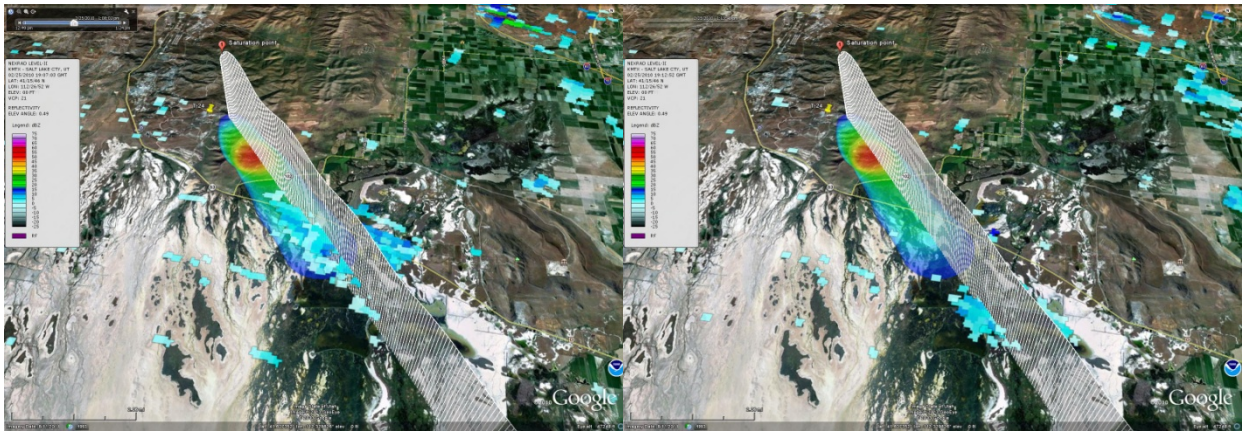

defined as a predicted trajectory that sharply deviated from the direction of travel shown by radar signatures. Caution was taken in comparing the predicted plume trajectory to radar signatures that showed a decrease in altitude over time. These scans are likely precipitation signatures falling to the ground and may transport away from the plume centerline.

Figure 7. Correlation of FSM-17 Radar Signatures with PlumeTracker Trajectory Showing a High Level of Correlation

Predicted D/P fields were compared to NEXRAD signatures, photographs, spotter observations, and neighborhood cleanup records. As with plume trajectories, correlations were grouped into levels of high, medium, and low. A high level of correlation was defined as a predicted D/P field that matches the relative intensities of NEXRAD reflectivity measurements and is confirmed by all other field data (**Figure 8**). A moderate level of correlation was defined as a D/P field that was slightly offset - too soon or too late - from reflectivity intensities and showed marked deviation from field records. A low level of correlation was defined as a D/P field that did not resemble radar reflectivity intensities or field data. Like plume trajectories, some caution had to be taken when comparing D/P field with radar reflectivity. PlumeTracker uses weather data starting at 6,000 ft mean sea level. As such, D/P fields are projected from generation in the cloud down to 6,000 ft. This may be anywhere from 1,000 to 2,000 ft above ground surface as the plume transports across adjacent terrain.

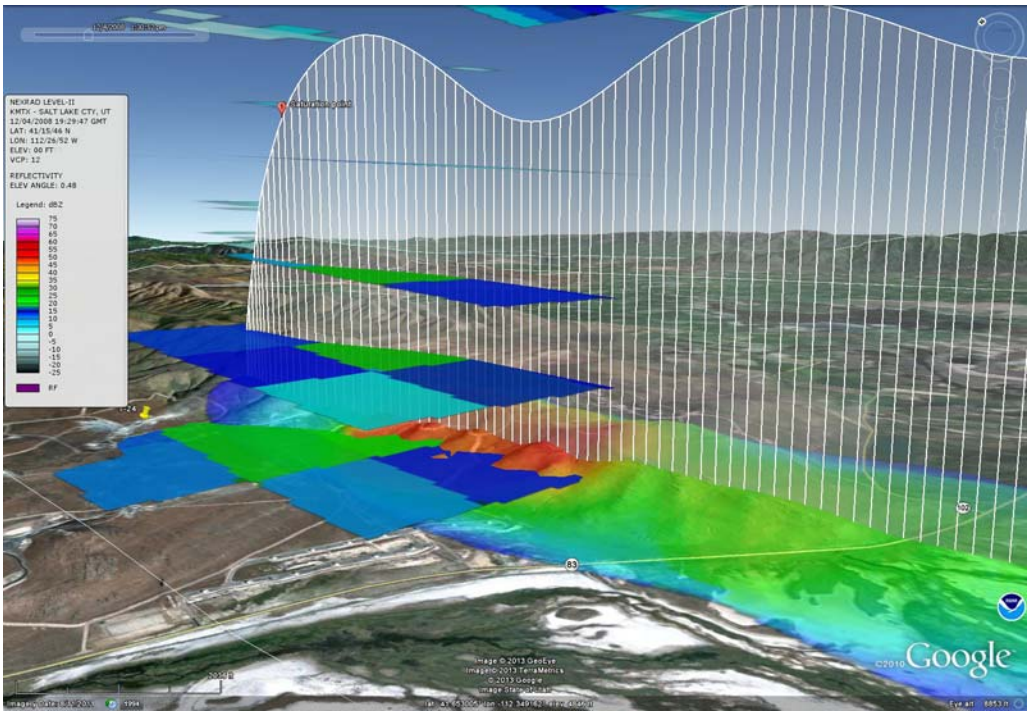

Figure 8. A High Level of Correlation between FSM-15 Reflectivity Intensity (green blocks) and the PlumeTracker Precipitation Field (red projection)

PlumeTracker satisfactorily predicted the track of all historical test fires in the dataset. All but one of the predicted tracks had a high level of correlation with NEXRAD signatures. The predicted track for TEM-12 deviated to the north of the collected NEXRAD signatures.

However, as shown in **Figure 9**, the NEXRAD signatures were predicted by the southern boundary of the computed dispersion tracks (blue lines).

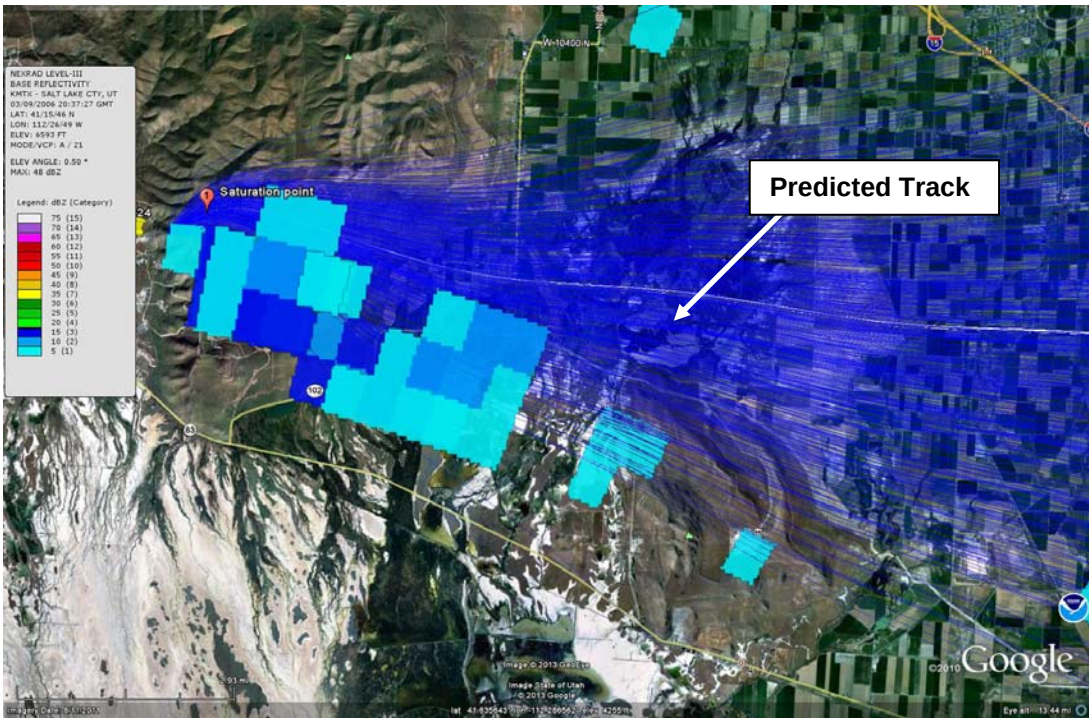

Figure 9. PlumeTracker Dispersions Tracks and NEXRAD Signatures for TEM-12

The deviation observed in the TEM-12 track may have been the result of using retroactive forecast data. Forecast data does not have the same resolution as radiosonde data and is usually based on soundings taken from Salt Lake City International Airport, approximately 65 miles from Promontory test facilities. Additionally, the soundings can be taken one to two hours prior to the static test. For the most part, this did not appear to pose a problem when generating PlumeTracker trajectories. However, TEM-12 may have occurred during a weather transition that was not captured in the retroactive forecast.

CONCLUSIONS

A software package, called PlumeTracker, capable of tracking the exhaust plume and the corresponding deposition and precipitation from large solid rocket motor tests has been developed and validated. The approach is physics-based and capable of predicting plume behavior for current test stand configurations. The model provides probabilities for plume trajectories and deposition fields based on the variability of the meteorological data. PlumeTracker was validated against twenty-three historical test fires to determine its ability to retroactively predict observed characteristics of each plume, specifically plume trajectory and precipitation fields. The dataset covered a variety of atmospheric conditions.

PlumeTracker satisfactorily predicted the D/P field of each historical test fire in the dataset. High correlation was found for all twenty-three of the historical firings. FSM-9, FVM-1, and FSM-12 were tested during meteorological conditions that did not promote a precipitation event. However, the dry deposition field projected by PlumeTracker closely matched the position and

duration of NEXRAD signatures that were more typical of a short-lived deposition event instead of rain formation and precipitation.

The results were used to estimate a statistical reliability based on the binomial distribution. A success was recorded when PlumeTracker accurately matched both plume track and precipitation field to at least a medium level of correlation. A low level of correlation was considered a failure. Based on the size of the dataset and no failures recorded during the analysis, PlumeTracker has an estimated reliability of 90% with 90% confidence. The ability to provide a more accurate understanding of plume behavior from static test motors provides ATK the opportunity to enhance their community partnership.

REFERENCES

1. Briggs, G.A., "A Plume Rise Model Compared with Observations", Journal of the Air Pollution Control Association", Vol. 15, No. 9, pp. 433-438, 1965
2. Briggs, G.A., "A Discussion on Recent Research in Air Pollution", *Philosophical Transations of the Royal Society of London. Series A, Mathematical and Physical Sciences*", Vol. 265, No. 1161, pp. 197-203, 1969
3. Briggs, G.A., "Some Recent Analysis of Plume Rise Observations", *Proc. Second Int. Clean Air Congress*, Academic Press, New York, 1971
4. Mills, M.T., "Modeling the Release and Dispersion of Toxic Combustion Products from Pool Fires", *Proceedings International Conference on Vapor Cloud Modeling*, Cambridge, MA, 1987
5. Fisher, B.E.A, Metcalfe, E., Vince, I., and Yates, A., "Modeling Plume rise and Dispersion from Pool Fires", *Atmospheric Environment*, Vol. 35, pp. 2101-2110, 2001
6. Cunningham, P. and Goodrick, S.L., "High-resolution Numerical Models for Smoke Transport in Plumes from Wildland Fires", *Remote Sensing and Modeling Applications to Wildland Fires*; Qu, J.J., Riebau, A., Yang, R., Sommers, W., Eds., pp. 74-88, Springer Publishing; New York, 2011
7. Achtemeier, G.L., "On Plume Rise – Matching Daysmoke with Briggs Equations for Industrial Stacks", Sixth Symposium on Fire and Forest Meteorology, October, 2005
8. Achtemeier, G.L., Goodrick S.A., Liu, Y., Garcia-Menendez, F., Hu,Y., and Odman, M.T., "Modeling Smoke Plume-Rise and Dispersion from Southern United States Prescribed Burns with Daysmoke", *Atmosphere*, Vol. 2, pp. 358-388, 2011
9. Liu, Y., Achtemeier, G.L., Goodrick, S., and Jackson, W.A., "Important Parameters for Smoke Plume Rise Simulation with Daysmoke", *Atmospheric Pollution Research*, Vol. 1, pp. 250-259, 2010
10. Bjorklund, J.R., Dumbauld, R.K., Cheney, C.S., and Geary, H.V., *User's Manual for the REEDM (Rocket Exaust Effluent Diffusion Model Computer)*, Salt Lake City, UT: H.E. Cramer Company Inc., 1982
11. Moreira, D.M., Trindade, L.B., Fisch, G., de Moraes, M.R., Dorado, R.M., and Guedes, R.L., "A Multilayer Model to Simulate Rocket Exhaust Clouds", *Journal of Aerospace Technology and Management,* Vol. 3, No. 1, pp. 41-52, 2011
12. Black, D.L. and Wells, J.E., "PlumeTracker Theory and User Manual", TR032512, January 2013

13. Wu, F. and Koh,R., “Mathematical Model for Multiple Cooling Tower Plumes”, Report No. KH-R-37, W.M. Keck Laboratory of Hydraulics and Water Resources, California Institute of Technology, July 1977
14. American Meteorological Society, Glossary of Meteorology, 2nd Edition (Electronic), http://amsglossary.allenpress.com/glossary/browse?s=m&p=51, “moist-adiabatic lapse rate definition”, 2000
15. Twomey, S., “The Nuclei of Natural Cloud Formation: The Supersaturation in Natural Clouds and the Variation of Cloud Droplet Concentrations”, Geofis, Pura Appl., Vol. 43, pp. 243-249, 1959
16. Grabowski, W.W., Andrejczuk, M., and Wang, L., “Droplet Growth in a Warm-rain Scheme with Twomey CCN Activation”, Atmospheric Research, Vol. 99, pp. 290-301, 2011
17. Rogers, R.R. and Yau, M.K., “A Short Course in Cloud Physics”, Elsevier, 1989
18. Tsai, P., *et al*. “Combined LiDar and Radar Observations of Smoke Plumes from Prescribed Burns”, *Proceedings of Fouth Symposium on LiDAR Atmospheric Applications*, Phoneix, AZ. 2009
19. Lavrov, A., *et al*. “Evaluation of Smoke Dispersion from Forest Fire Plumes Using LiDar Experiments and Modeling”, INT J THERM SCI. 848-859. 2006
20. Wold, C.E., *et al*. “Validation of Smoke Plume Rise Models Using Ground-Based LiDar”, *Proceedings of 3rd Fire Behavior and Fuels Conference.* Spokane, WA, 2010
21. Evans, R.J., “Delta II Explosion Plume Analysis Report”, NASA Contractor Report. NASA/CR-2000-208582. 2000
22. National Oceanic and Atmospheric Administration, National Climatic Data Center (NCDC), http://www.ncdc.noaa.gov/nexradinv/
23. National Oceanic and Atmospheric Administration, National Climatic Data Center (NCDC), http://www.ncdc.noaa.gov/oa/wct/
24. Thiokol Corporation, Environmental Permits Strategic Division, “Plume Characterization: 10 March 1994 Test Firing.” 1994

Development and Validation of a Computational Model for Predicting the Behavior of Plumes from Large Solid Rocket Motors

Jason E. Wells
Environmental Services
(435) 863-6895
Jason.Wells@atk.com

ATK Technical Symposium
April 24-25, 2013

Distribution A: Approved for public release; distribution is unlimited
This work was performed under NASA Contract No: NNM07AA75C MOD 95FWD

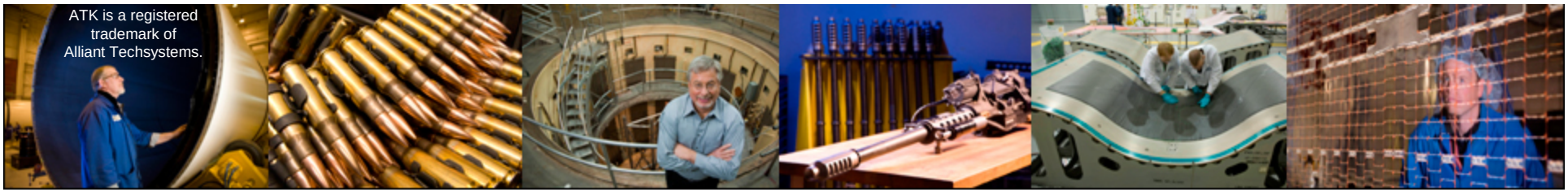

Acknowledgements

David Black – Fluid Dynamics

Casey Taylor – Composite Structures

Daron Isaacs – Engineering Tools and Processes

Lynn Walker – Environmental Services

Introduction

Problem Description

- Particulate loading
- Particulate deposition

Objectives

- Predict plume direction
- Predict debris deposition field
- Utilize as a tool to assess plume mitigation strategies

PlumeTracker Model

- Model description
- Model validation

Problem Description

- Plume is composed of motor exhaust and surrounding debris
- Plume rises to condensation point and forms cloud
- Cloud is transported by upper level winds and eventually precipitates

Particulate Loading

Particulate Deposition

PlumeTracker Model

Physical Phenomena

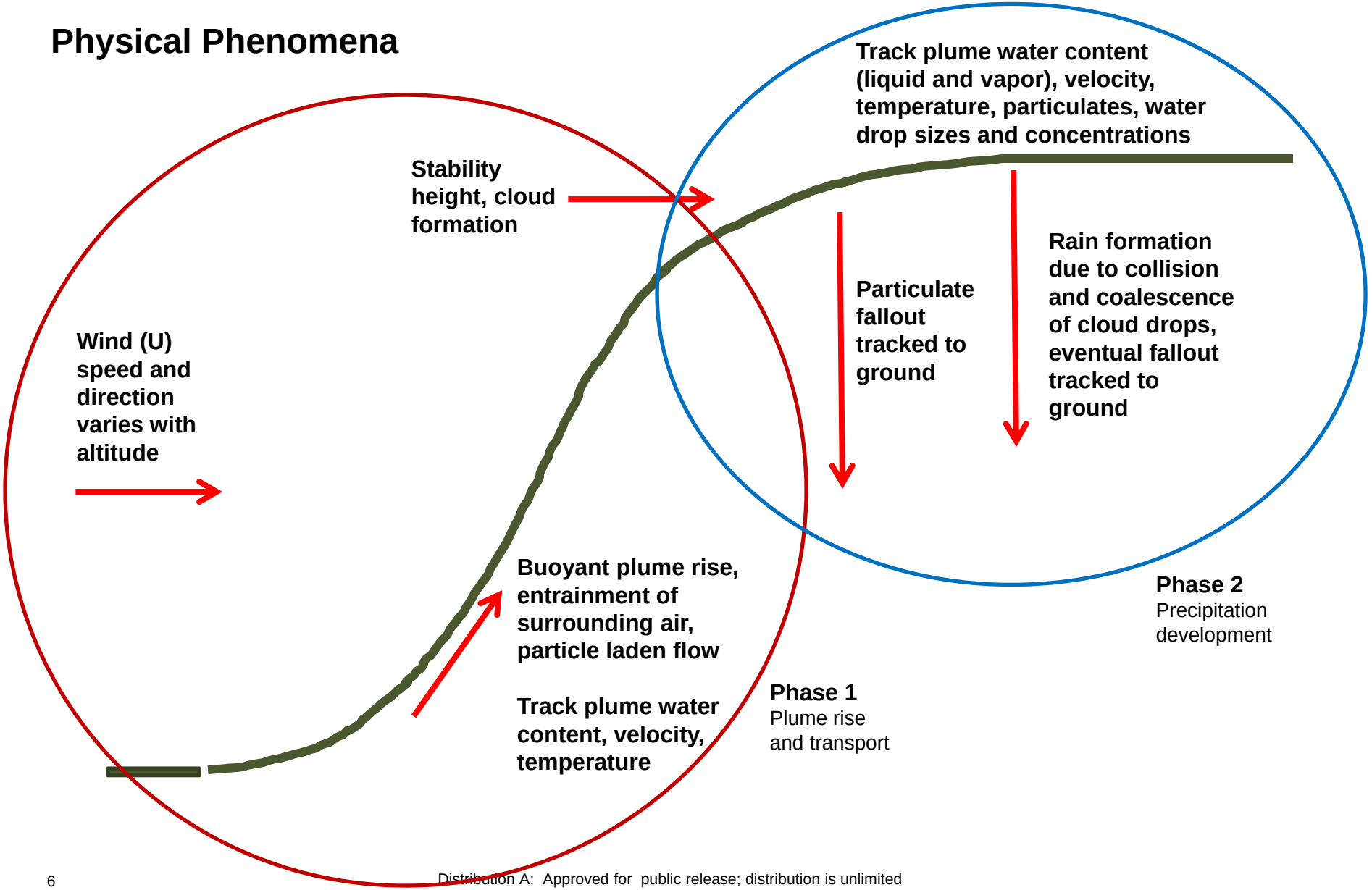

PlumeTracker Model

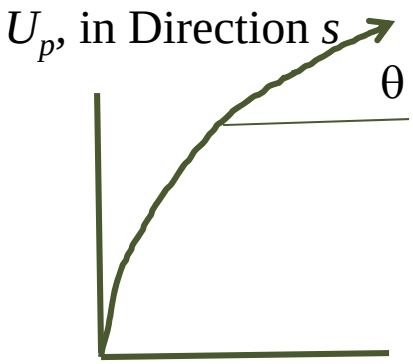

Vertical Plane

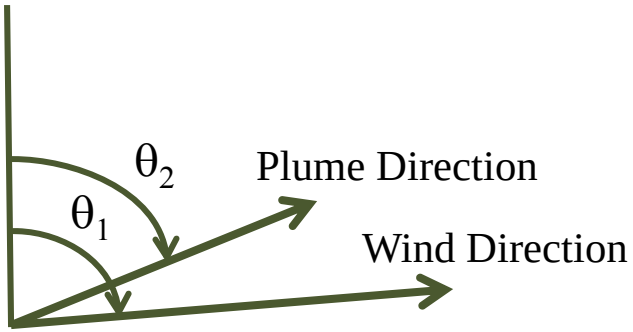

Horizontal Plane

- Equations written in plane of plume motion
- Three-dimensional tracking
  1. Horizontal in plume direction
  2. Horizontal perpendicular to plume direction
  3. Vertical

PlumeTracker Model

Buoyant Plume Rise and Stability

1. Initial conditions defined by CFD model
2. Plume location and altitude tracked through solving the conservation equations for mass, momentum, and energy

Entrainment velocity

Drag force – wind acting on plume

Mass

$$\frac{d(A\rho_p U_p)}{ds} = \rho_a 2\pi r U_{ent}$$

Momentum

$$\frac{d(A\rho_p U_{p'}^2)}{ds} = \rho_a U_\infty \sin(\theta_1 - \theta_2) 2\pi r U_{ent} + \frac{1}{2} C_d \rho_a \left[U_\infty \sin(\theta_1 - \theta_2)\right]^2 r$$

$$\frac{d(A\rho_p U_p^2 \cos\theta)}{ds} = \rho_a U_\infty \cos(\theta_1 - \theta_2) 2\pi r U_{ent} + \frac{1}{2} C_d \rho_a \left[U_\infty \cos(\theta_1 - \theta_2) \sin\theta\right]^2 r |\sin\theta|$$

Momentum of entrained air

$$\frac{d(A\rho_p U_p^2 \sin\theta)}{ds} = gA(\rho_a - \rho_p(1-\sigma_p)) + \frac{1}{2} C_d \rho_a \left[U_\infty \cos(\theta_1 - \theta_2) \sin\theta\right]^2 r \cos\theta$$

Energy

$$\frac{d\left[(T_p - T_a)U_p\right]}{ds} = -\left(\frac{dT_a}{dz} + \Gamma\right) U_p \sin\theta$$

Mixing of entrained ambient air

Lapse rate

PlumeTracker Model

Starts When Some Part of Plume Supersaturates

1. Activate nuclei (at each time step)
2. Separate into sizes
3. Allow growth to cloud and rain droplets

$$N_{ccn} = C(100S)^k \qquad C=4000,\ k=2\ (\text{dirty air})$$

$$\Delta N = C(100S)^k - C(100S_{\max})^k$$

Twomey relationship for activated (capable of growth) droplets

$$r_{act} = \frac{2}{3}\frac{A}{S}, A = \frac{2M_w\sigma_w}{RT\rho_w}$$

Calculates number and size of water in droplets

$$\frac{dR}{ds} = \frac{\xi_1(S-1)}{R}, \xi_1 = growth\ parameter$$

Condensational growth

$$\frac{dR}{ds} = \frac{\pi}{3}\int_0^R \left(\frac{R+r}{R}\right)^2 [u_R - u_r] N_r r^3 E_{R,r} dr$$

Collusional growth

PlumeTracker Model

Wet and Dry Particle Fallout

Group into discrete size bins

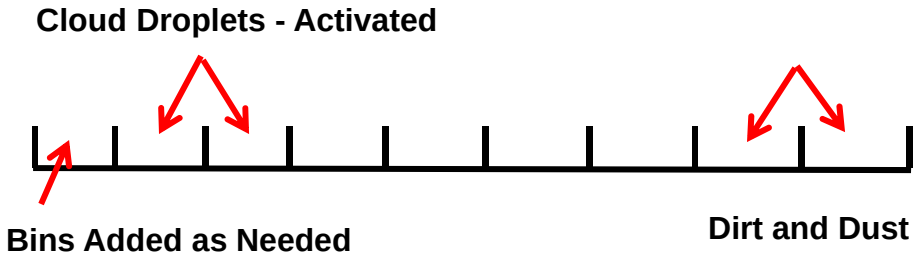

Each bin tracks

- **Size (can grow in time if S>0)**
- **Number**
- **Mass**
- **Fall velocity U_f**
- **Time**

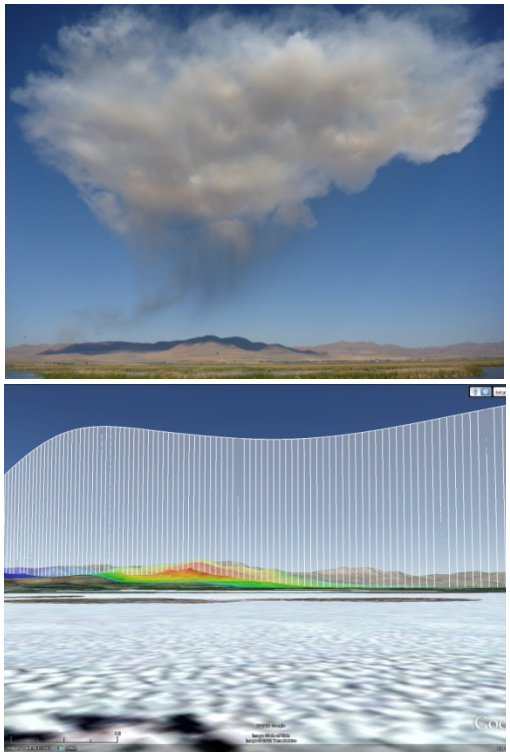

Carried by plume until $\int_0^t (U_p - U_f)dt = \sqrt{\frac{A_p}{\pi}}$

Then bin is tracked to ground and fallout pattern estimated

Dirt and dust particle allowed to grow when S>1; assume particles are wet and grow like cloud/rain droplets

PlumeTracker Validation: Data

Weather Data from 23 RSRM/RSRMV Static Tests

- Retroactive forecast
- On-site radiosonde data
- Variety of conditions represented

Plume Observation Data

- NEXRAD from Salt Lake and Pocatello
- Field observations (e.g., photographs, video, cleanup maps)

Test Date	Test ID	Test Stand
March 10, 1994	FSM-4	T-24
November 9, 1995	FSM-5	T-24
April 24, 1997	FSM-6	T-97
June 24, 1998	FSM-7	T-97
February 17, 2000	FSM-8	T-97
May 24, 2001	FSM-9	T-97
November 1, 2001	ETM-2	T-24
January 23, 2003	FSM-10	T-24
October 23, 2003	ETM-3	T-97
June 10, 2004	FSM-11	T-97
February 17, 2005	FVM-1	T-24
August 16, 2005	PRM-1	T-97
March 9, 2006	TEM-12	T-24
April 28, 2006	FSM-12	T-97
November 16, 2006	FSM-13	T-97
May 24, 2007	FSM-14	T-97
November 1, 2007	TEM-13	T-24
May 1, 2008	FVM-2	T-24
December 4, 2008	FSM-15	T-24
September 10, 2009	RSRMV DM-1	T-97
February 25, 2010	FSM-17	T-24
August 31, 2010	RSRMV DM-2	T-97
September 8, 2011	RSRMV DM-3	T-97

PlumeTracker Validation: FSM-17

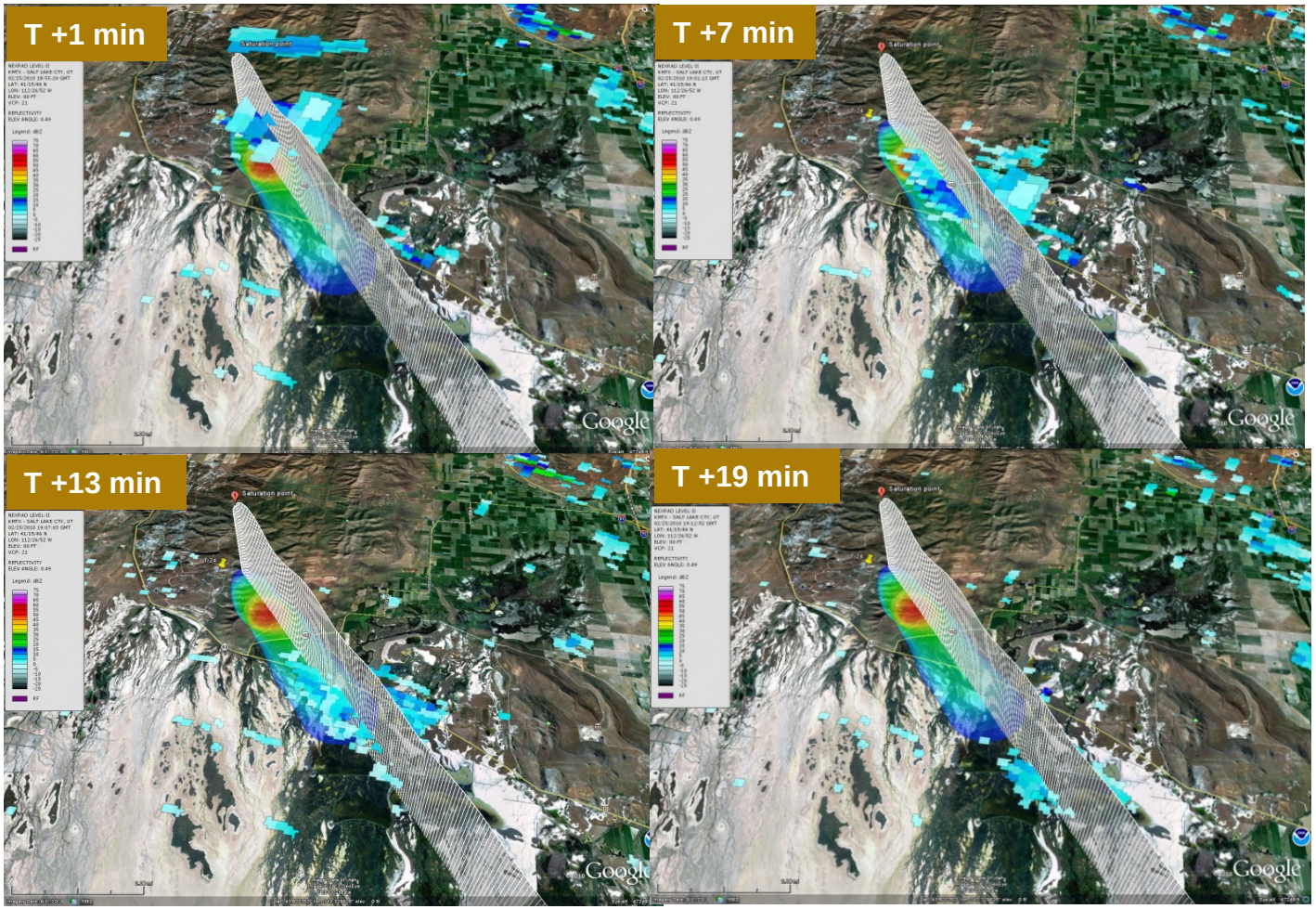

PlumeTracker Trajectory Showing High Level of Correlation with FSM-17 Radar Signatures

PlumeTracker Validation: DM-1

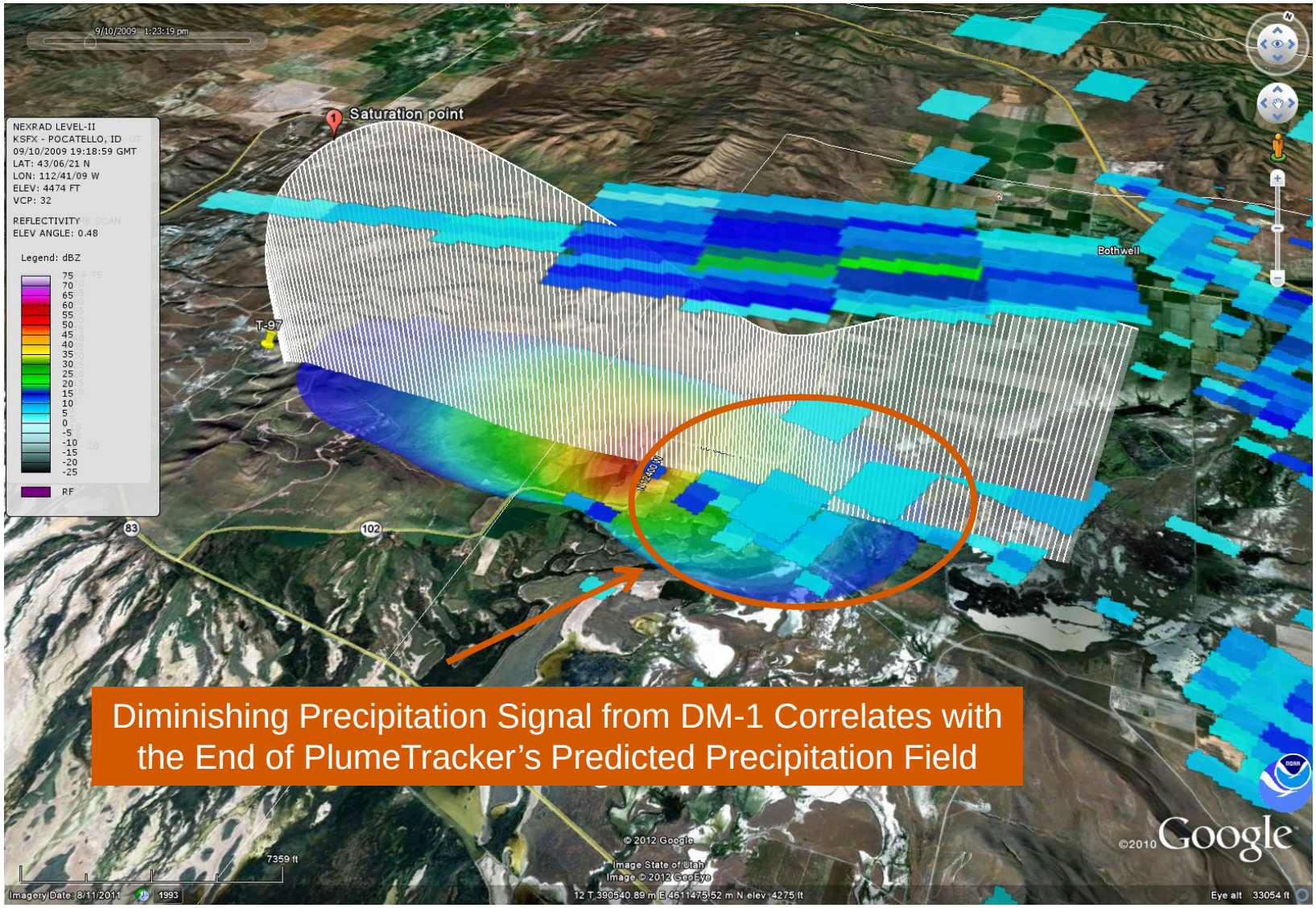

PlumeTracker Results: DM-2

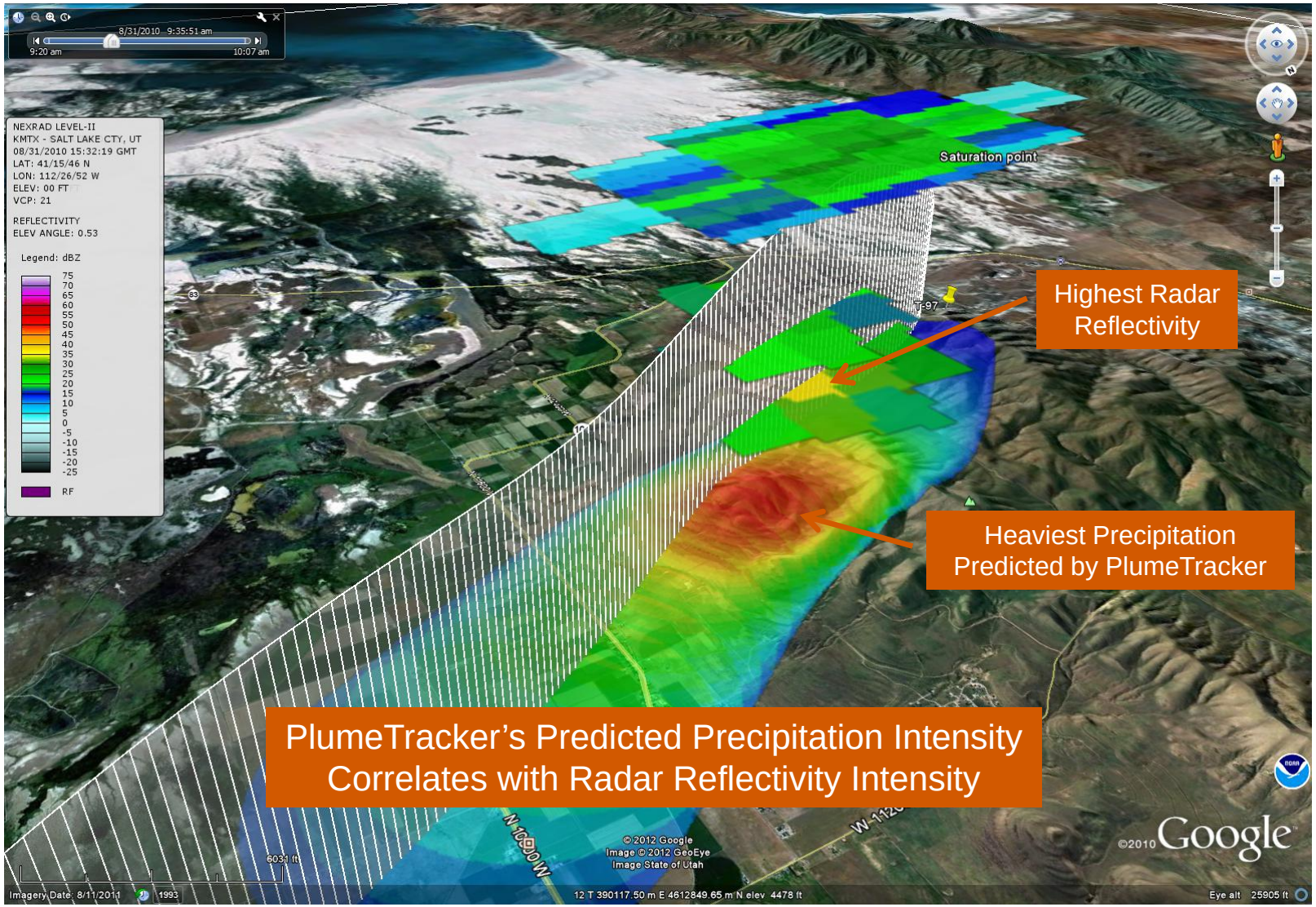

PlumeTracker Results: TEM-12

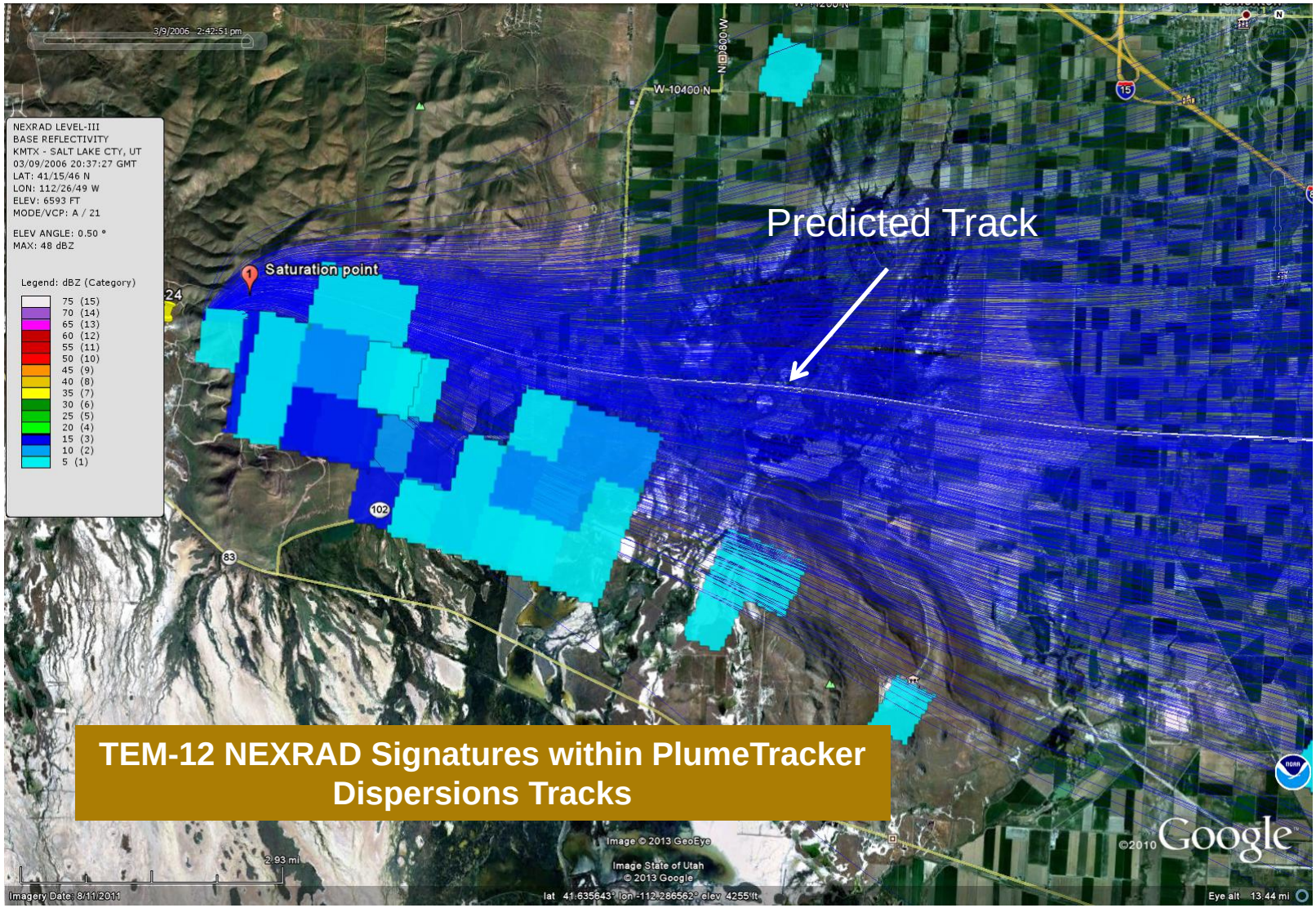

PlumeTracker Validation

Plume Trajectory Correlation

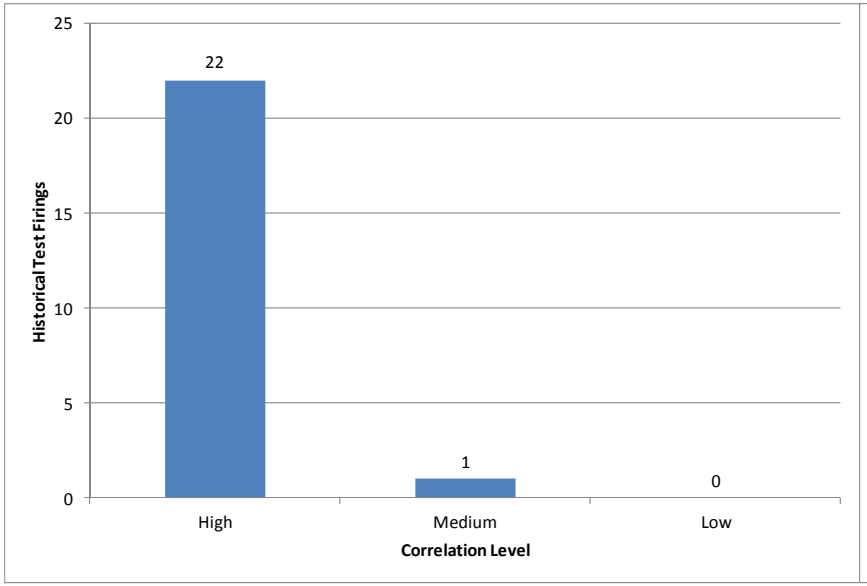

Plume Deposition Correlation

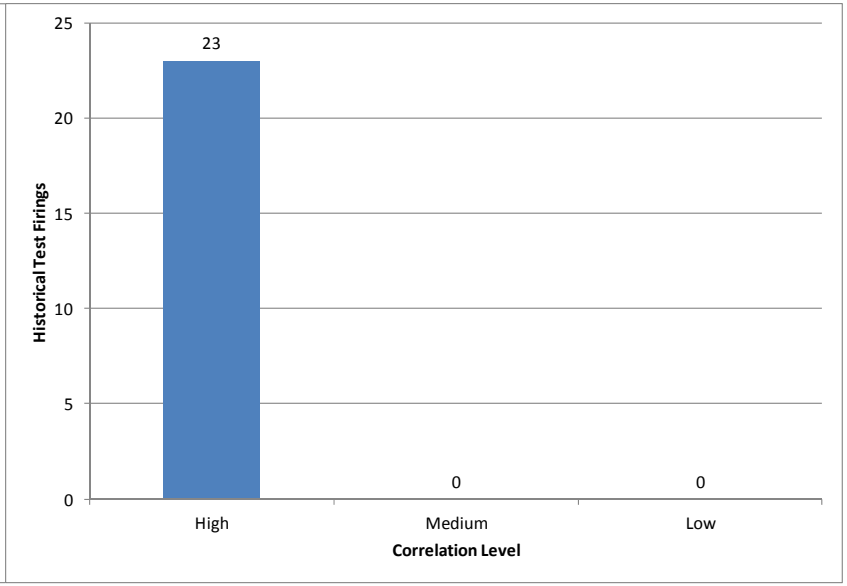

- Statistical reliability estimated using binomial distribution
- High/medium correlation = success
- Low correlation = failure
- Based on size of dataset and 0 recorded failures:

90% success with 90% confidence

Summary

PlumeTracker

- Physics-based predictive tool for motor plumes
  - Predicts plume trajectories and dry/wet deposition events
- Good agreement with plume trajectory and precipitation fields of 23 historical motor firings

PlumeTracker provides a tool to:

- Predict behavior of static test plumes
- Analyze mitigation strategies
- Assess potential risks that might arise from testing new motors